Photoelectron Circular Dichroism as a Signature of Subtle Conformational Changes: The Case of Ring Inversion in 1-Indanol

Jennifer Dupont, Valéria Lepère, Anne Zehnacker, Sebastian Hartweg, Gustavo A Garcia, Laurent Nahon

Photoelectron Circular Dichroism as a Signature of Subtle Conformational Changes: The Case of Ring Inversion in 1-Indanol

Jennifer Dupont,[a)] *Valéria Lepère,*[a)] *Anne Zehnacker*[a)]*

Sebastian Hartweg[b)] *Gustavo A. Garcia,*[b)] *Laurent Nahon*[b)]*

a) Institut des Sciences Moléculaires d'Orsay (ISMO), CNRS, Université Paris-Saclay, F-91405 Orsay, France

b) Synchrotron Soleil, L'Orme des Merisiers, St. Aubin BP48, F-91192 Gif sur Yvette, France

Corresponding Authors

* Anne Zehnacker anne.zehnacker-rentien@universite-paris-saclay.fr * Laurent Nahon laurent.nahon@synchrotron-soleil.fr

ABSTRACT: Chirality plays a fundamental role in the molecular recognition processes. Molecular flexibility is also crucial in molecular recognition, allowing the interacting molecules to adjust their structures hence optimize the interaction. Methods probing simultaneously chirality and molecular conformation are therefore crucially needed. Taking advantage of a possible control in the gas phase of the conformational distribution between the equatorial and axial conformers

resulting from a ring inversion in jet-cooled 1-indanol, we demonstrate here the sensitivity of valence-shell photoelectron circular dichroism (PECD) to both chirality and subtle conformational changes, in a case where the photoelectron spectra of the two conformers are identical. For the highest occupied orbital, we observe a dramatic inversion of the PECD-induced photoelectron asymmetries, while the photoionization cross-section and usual anisotropy (β) parameter are completely insensitive to conformational isomerism. Such a sensitivity is a major asset for the ongoing developments of PECD-based techniques as a sensitive chiral (bio-)chemical analytical tool in the gas phase.

TOC GRAPHICS

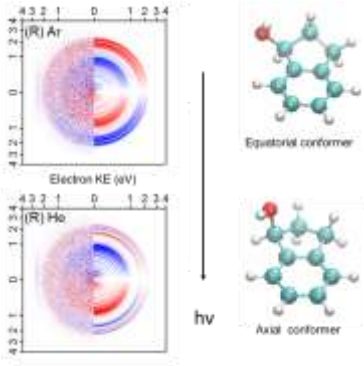

KEYWORDS Chirality – Conformational Isomerism – Indanol – Circular Dichroism – Photoionization –Velocity Map Imaging

Chiroptical spectroscopy techniques, *i.e.* spectroscopy sensitive to chirality, are widely used to characterize the structure of biomolecules.[1] Besides being a signature of the absolute configuration of a chiral molecule, they show in general a high sensitivity to molecular conformation. Thereby, electronic circular dichroism (ECD), the difference in absorption between left- and right-handed circular polarized light (CPL), is a powerful means for studying the secondary structure of biomolecules like proteins or DNA derivatives.[2-3] In the IR range, its vibrational counterpart, vibrational circular dichroism (VCD), is strongly influenced by conformational isomerism and molecular interactions.[4-10]

Despite their broad applications, these methods suffer from a lack of sensitivity and the measured effect is limited to ~10^{-3} of the total absorption for ECD and even less, down to 10^{-5}, for VCD. In practice the weakness of ECD makes extremely challenging its application to dilute matter in the gas phase, in particular under jet-cooled or cryogenic ion trap conditions.[11-13]

In contrast, the recently introduced Photoelectron Circular Dichroism (PECD) is ideally suited for studying gas-phase molecules.[14-16] PECD is observed as a forward-backward asymmetry in the photoelectron angular distribution with respect to the light axis for randomly oriented chiral molecules photoionized by CPL. Unlike the abovementioned chiroptical spectroscopy methods, it is allowed in the electric dipole approximation, which explains its intense relative magnitude, reaching up to almost 40 % of the average photoelectron intensity obtained with left and right CPL.[17] The normalized one-photon photoionization angular distribution function $I^{\{p\}}(\theta)$ is written as:

$$I^{\{p\}}(\theta) = 1 + b_1^{\{p\}} P_1(\cos\theta) + b_2^{\{p\}} P_2(\cos\theta) \qquad \text{(Eq 1)}$$

where P_1 and P_2 are the first and second Legendre polynomial, p is characteristic of the light polarization, with p= 0, +1, and -1 for linear, right- and left-handed circular polarizations,

respectively, and θ is the angle of electron emission with respect to the photon axis. The $b_2^{\{\pm 1\}}$ coefficient equals $-1/2\,\beta$, where $\beta = b_2^{\{0\}}$ is the usual (achiral) anisotropy parameter in photoionization. The so-called dichroic b_1 coefficient vanishes for linear polarization or non-chiral molecules. For chiral molecules, $b_1^{\{1\}} = -b_1^{\{-1\}}$, so that opposite effects are observed for right- and left-handed CPL, as expected for all chiroptical spectroscopy techniques. Opposite effects are also observed for the two enantiomers of a chiral molecule. The sign and the magnitude of PECD depends on the orbital (highest occupied orbital (HOMO), HOMO -1 etc.) from which the photoelectron is ejected. It is also a final state dynamical effect (depending on the kinetic energy of the outgoing photoelectron) originating from the scattering of the photoelectron by an intrinsically asymmetric potential. PECD appears as a delicate probe of the molecular potential, very sensitive to static (isomers, conformers) and dynamic (vibrational) structural effects, as well as clustering.[15-16] Besides its potential applications in astrochemistry,[16, 18-19] analytical purposes,[20-23] or chemical dynamics,[24-25] it is a powerful tool for probing molecular chirality and conformational flexibility at the same time[26] as well as their interplay.[27] The high sensitivity of PECD to conformational isomerism has been recently exemplified by the study of proline[18] in which the steric bias induced by the pyrrolidine ring results in two families of conformers, differing in their H-bond pattern and related by the ring inversion motion. They strongly differ in their ionization energy of the highest occupied molecular orbital (HOMO). This difference allowed assessing directly the relative contribution of the two families by ionizing their HOMO orbital and comparing the b_1 values extracted at different electron kinetic energies. A conformer-dependent PECD has also been reported from conformation-dependent dissociative ionization channels in gas phase serine.[28]

The present work focuses on the role of inversion motion on PECD, on the example of 1-indanol for which ring-inversion conformers can be advantageously isolated under supersonic expansion conditions. 1-indanol (Figure 1) is a chiral aromatic alcohol composed of a benzene ring fused with a five-membered alicyclic ring bearing the hydroxyl substituent. Under supersonic-jet conditions, its S_0-S_1 electronic spectrum strongly depends upon the carrier gas and shows an additional transition when helium or neon are used instead of argon.[29-31] Conformer-specific vibrational spectroscopy clearly indicated that this additional transition is due to a higher-energy conformer. [32] The observed conformers were assigned to the equatorial and axial conformations of the hydroxyl substituent, based on the comparison between their experimental conformer-selective IR spectra and that simulated by quantum chemical calculations. The equatorial conformer, denoted as 1eq, indeed has a slightly lower ν(OH) stretch vibrational frequency than the axial form, denoted as 2ax.[32] It is also more stable by a value ranging from 0.2 kJ/mol at the MP2/aug-cc-pVTZ level to 1.3 kJ/mol at the CCSD(T)/aug-cc-pVTZ level. The proposed structures were recently confirmed by high-resolution spectroscopy.[33] The barrier for interconversion was not determined for 1-indanol, but is calculated at 8 to 10 kJ/mol at the MP2/6-31G(d,p) level for the related molecules indan or 2-indanol, a value at the verge of what can be overcome under supersonic jet conditions.[34] In helium, kinetic trapping results in separate trapping of each conformer in its own potential well, while relaxation towards the most stable form is favored in heavier carrier gases. As a result, the most stable equatorial form is the only one present in argon. Changing the carrier gas is therefore a means to control the ratio between the inversion isomers, with an experimentally observed axial/equatorial ratio varying from 0 in argon to ~ 1/3 in helium. This property offers the first opportunity of directly observing and controlling the PECD behavior of a flexible molecule in conditions where only one isomer or two are present. Here we show that

1-indanol is a perfect proxy to template the exquisite conformational sensitivity of PECD, in a case where, unlike proline, the photoelectron spectrum (PES) of the two conformers are genuinely superimposable.

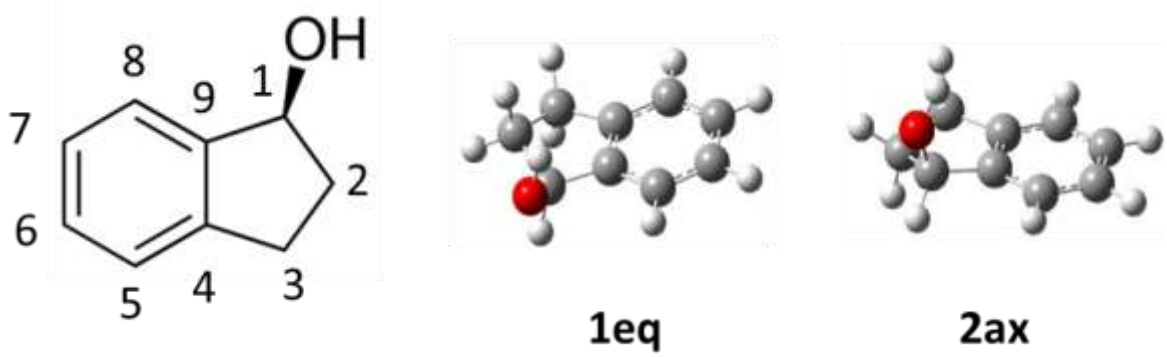

Chart 1. Structure of (S) (+) 1-indanol and carbon atoms numbering (left). Most stable equatorial (1eq) and axial (2ax) conformers (right) calculated at the MP2/6-31G++(d,p) level.

Mass spectra

The mass spectra, recorded at a photon energy of 9 and 12 eV, are shown in Figure S1 of the supporting information (SI). At 9 eV, only the parent molecule (*m/z* 134) is observed. The mass spectrum recorded at 12 eV shows the appearance of a fragment (*m/z* 133). It corresponds to hydrogen loss, a process frequently encountered in photo-generated cations of aromatic molecules.[35 36] No other fragment than *m/z* 133 is detected between 9 and 12 eV.

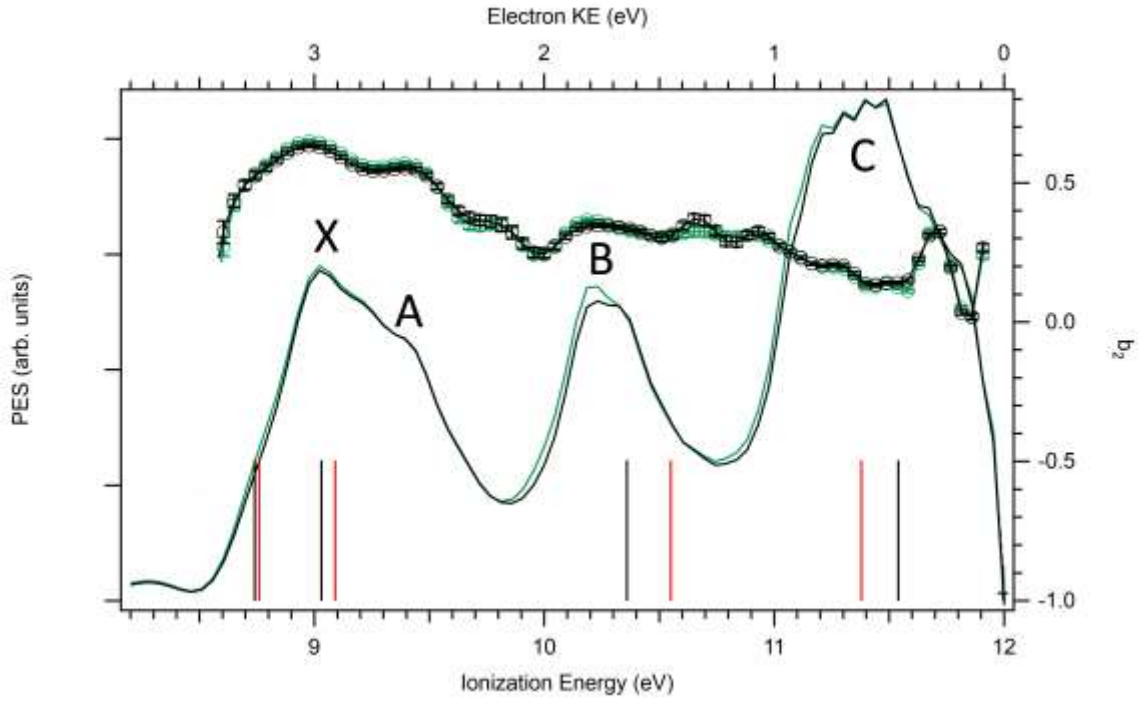

Figure 1: PES (solid line) and b_2 parameters (open circles) as a function of the ionization energy using helium (green) and argon (black) as a carrier gas, recorded at 12 eV photon energy and obtained by summing the signal at *m/z* 134 and *m/z* 133. KE is the kinetic energy of the electrons, defined as the difference between the photon energy and the ionization energy. The main peaks of the PES are denoted by X, A, B, C. The orbital energies are shown for the equatorial (black sticks) and axial (red sticks) conformers. The b_2 values obtained for a PES intensity smaller than 10% of the maximum intensity are not shown.

Photoelectron spectra

Figure 1 displays the PES of the *(S)* enantiomer recorded at a photon energy of 12 eV, and obtained by summing the electrons in coincidence with the ions at *m/z* 134, *i.e.* the parent 1-indanol, and those at *m/z* 133, *i.e.* the fragment resulting from H loss. The PES obtained at 11 eV is shown in Figure S2 of the SI. The PES are strikingly identical within our resolution (~100 meV) whether

helium or argon is used as a carrier gas, as are the higher resolution (~20 meV) threshold photoelectron spectra (TPES) shown in Figure S3 of the SI. The TPES yields an experimental ionization energy of ~ 8.6 eV, in good agreement with the adiabatic ionization energy (IE_{ad}) calculated with the Outer Valence Green Functions (OVGF) method, namely, 8.74 and 8.76 eV for the equatorial and axial conformers, respectively. The values at the B3LYP-D3BJ/6-31++G(d,p) and those at the MP2/6-31++G(d,p) levels are collected in Table S1 of the SI. Similar values of the adiabatic ionization energy have been measured for the related achiral molecule 2-indanol, namely, 8.55 and 8.50 eV for the equatorial and axial conformers, respectively,[37] which substantiates the theoretical values obtained here. The calculated vertical ionization energy (IE_{ve}) is ~0.5 eV higher than the adiabatic one (see Table S1), at both levels of theory. This is consistent with the measured width of the first PES band. Whatever the modelling, the energetics of the two conformers are very close. The similitude in both adiabatic and vertical calculated ionization energies at all levels of theory, and the overall PES shape as seen shown in Figure 1 and S3, clearly precludes the observation of any different signature for 1eq and 2ax by the sole PES observable.

Four peaks appear below 12 eV in the PES, denoted as X, A, B, C in what follows. They were fitted by a set of Gaussian functions with peak maxima located at 8.91, 9.27, 10.26 and 11.41 eV, respectively (see Section 3 of the SI). These peaks can be assigned to the three highest occupied orbitals, the OVGF calculated energy of which is also given in Figure 1 for the sake of comparison. Figure 2 shows the electron density distribution corresponding to the three highest occupied orbitals. In particular, the HOMO and HOMO-1 are described as π orbitals located on the aromatic ring, and both show little difference between the axial and equatorial conformers. The HOMO energy is calculated at 8.74 and 8.76 eV and that of the HOMO-1 at 9.03 and 9.09 eV for the equatorial and axial conformers, respectively, in good agreement with the experimental X and A

bands. Ionizing the π orbitals does not lead to fragmentation; only the parent at *m/z 134* is observed below 9.7 eV. Peak B at 10.26 eV is assigned to the HOMO-2, corresponding to the ionization of the lone pair of the oxygen atom, with contribution of the C_2C_3 σ orbitals and the C_1H σ orbital. The calculated energies are again in satisfactory agreement with the experiment, at 10.36 and 10.55 eV for 1eq and 2ax, respectively. Excitation of the HOMO-2 also corresponds to the onset for hydrogen loss at 9.7 eV (see the disappearance of the parent cations above this energy in Figure S4), which can be accounted for by the contribution of the C_1H σ orbital to HOMO-2. Peak C at 11.41 eV is assigned to HOMO-3, which contains contributions of the oxygen lone pair n_O as well as the C_1C_2 σ orbitals. Its calculated energy is similar for 1eq and 2ax (11.54 and 11.38 eV, respectively), and close to the value of Peak C. Despite a globally satisfactory agreement, the calculated and observed value slightly differ from each other. The vibrational spectrum of jet-cooled radical cations of primary alcohols produced by VUV ionization has been interpreted in terms of strong hyperconjugation effects between the singly-occupied orbital n_O and the adjacent CC and CH orbitals.[38] Such an effect could be at play here as well and not well accounted for in the calculations, which would explain the slight difference between the experimental and calculated data. Comparison between the mass-selected PES recorded at *m/z* 134 and *m/z* 133 indicates that the excited state of the ion achieved upon ionization of HOMO-3 is unstable and hydrogen loss becomes dominant at this energy (see Figure S4).

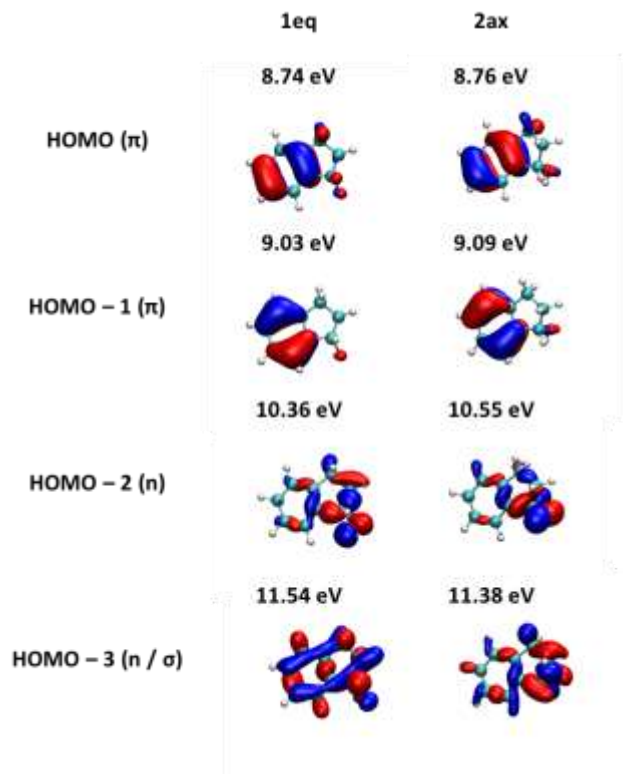

Figure 2: Electron density of the four highest occupied orbitals calculated at the MP2/6-31G++(d,p) level. The orbital energies are those calculated at the OVGF/cc-pVTZ level using the MP2 geometries.

Figure 1 also shows the b_2 parameters across the PES, exhibiting, as expected, some variations with the binding energy, *i.e.* with the final electronic state of the cation. Like the PES (partial cross section), the b_2 parameter (equivalent to β) is identical for the two conformations within the error bar across the four cation electronic states, reflecting the limited sensitivity of this observable to the molecular structure and the resulting electronic structure changes.

Photoelectron Circular Dichroism (PECD)

The PECD spectra have been recorded both in helium and in argon for photon energies between 9 and 12 eV. We will discuss in detail the data recorded at a photon energy of 11 eV, which are the

most telling. Figures 3(a-d) show the parent mass-selected raw difference images, corresponding to the difference between left CPL (LCPL) and right CPL (LCPL), denoted as (LCPL-RCPL), as well as the Abel-inverted images recorded for both enantiomers seeded in each of the carrier gases, obtained at a photon energy of 11 eV. The images clearly show the forward/backward asymmetry in the angular distribution of the electron, which is proportional to cosine of the ejection angle and is the signature of PECD, as well as a mirroring between *(R)* and *(S)* enantiomers, as expected. The images already offer a visual overview of the marked disparities appearing when changing the carrier gas, which are quantified in the corresponding photoelectron (PES) and PECD spectra shown in Figures 3(e-f) as a function of the electron kinetic energy. The maximum magnitude of the PECD is of the order of 6 % (b_1 =0.03). The measured PECD confirms the quasi-perfect mirroring within errors bars between the two enantiomers and exhibits a striking difference between He and Ar. In Ar, b_1 is of constant sign up to 9.5 eV, *i.e.* for the ionization of the HOMO and HOMO-1, then changes sign upon ionization of HOMO-2. Moreover, it shows a clear electron kinetic energy dependence, in particular some oscillations within the same electronic band which could correspond to vibronic transitions, as evidenced for the showcase molecule methyloxirane.[39] This is consistent with the geometry change upon ionization, shown in Figure S8.

The difference between the Ar and He cases is striking for the ionization of the HOMO, where a change in sign is observed when going from argon to helium. These results show that the b_1 parameters of the axial and equatorial conformers are opposite in sign. Moreover, the concentration of the equatorial conformer being larger than that of the axial conformer, the PECD of the latter must be larger in magnitude to account for the change in sign. In more quantitative terms, we can assume that the ratio 2ax/1eq is similar to that previously determined under similar experimental conditions using a continuous nozzle and amounts to 1/3 in helium.[30] On the basis of this value,

the experimental results lead to the conclusion that the PECD of 2ax is about four time larger in magnitude than that of 1eq. Concerning the HOMO-1 orbital, the effect is less striking but still present. No change of sign is observed there, but the b_1 parameter is weaker in He over the whole HOMO-1 energy range. This indicates again an opposite sign for the axial and equatorial conformers. The differences between Ar and He are more discrete in the region of the HOMO-2 orbitals. The overall magnitude of b_1 is similar with the two carrier gases, pointing towards similar properties of the two conformers in this binding energy range.

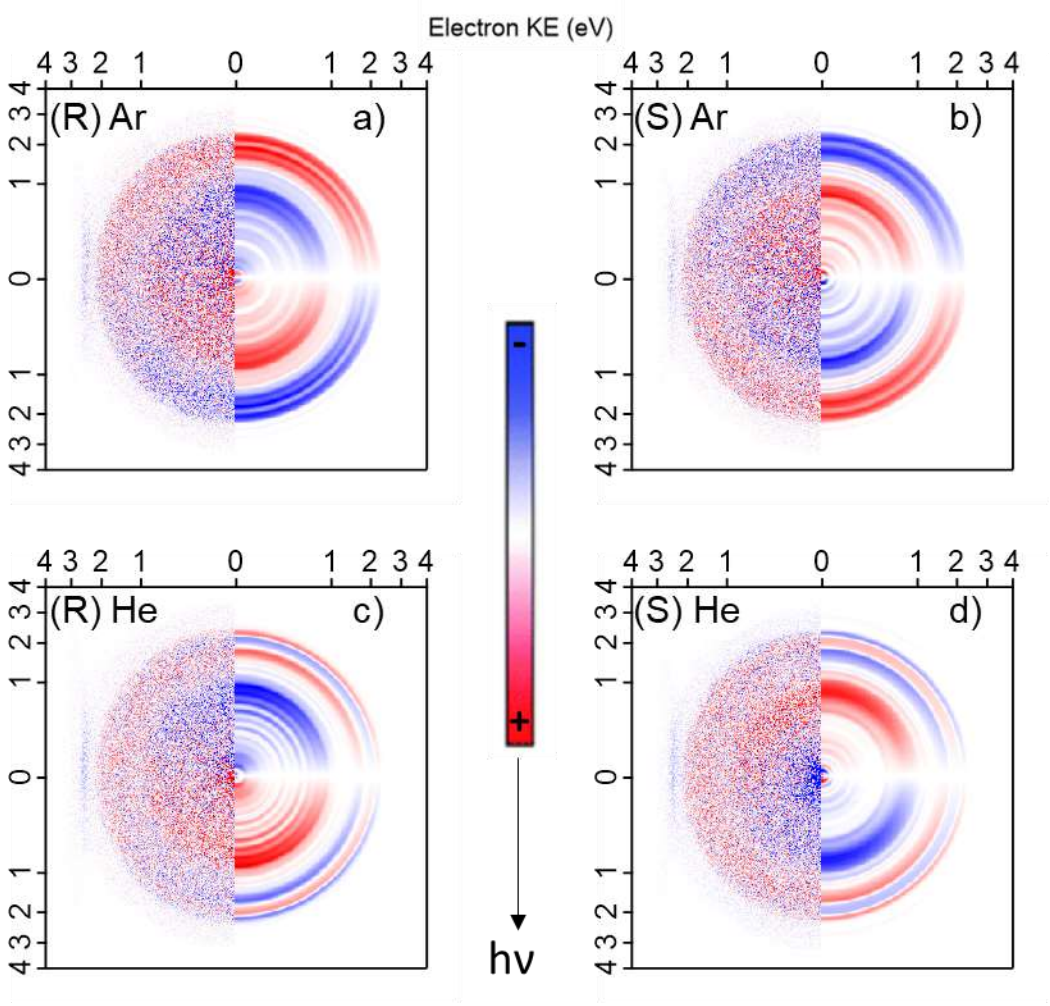
Electron KE (eV)
(R) Ar
a)
(S) Ar
b)
(R) He
c)
(S) He
d)
-
+
hv

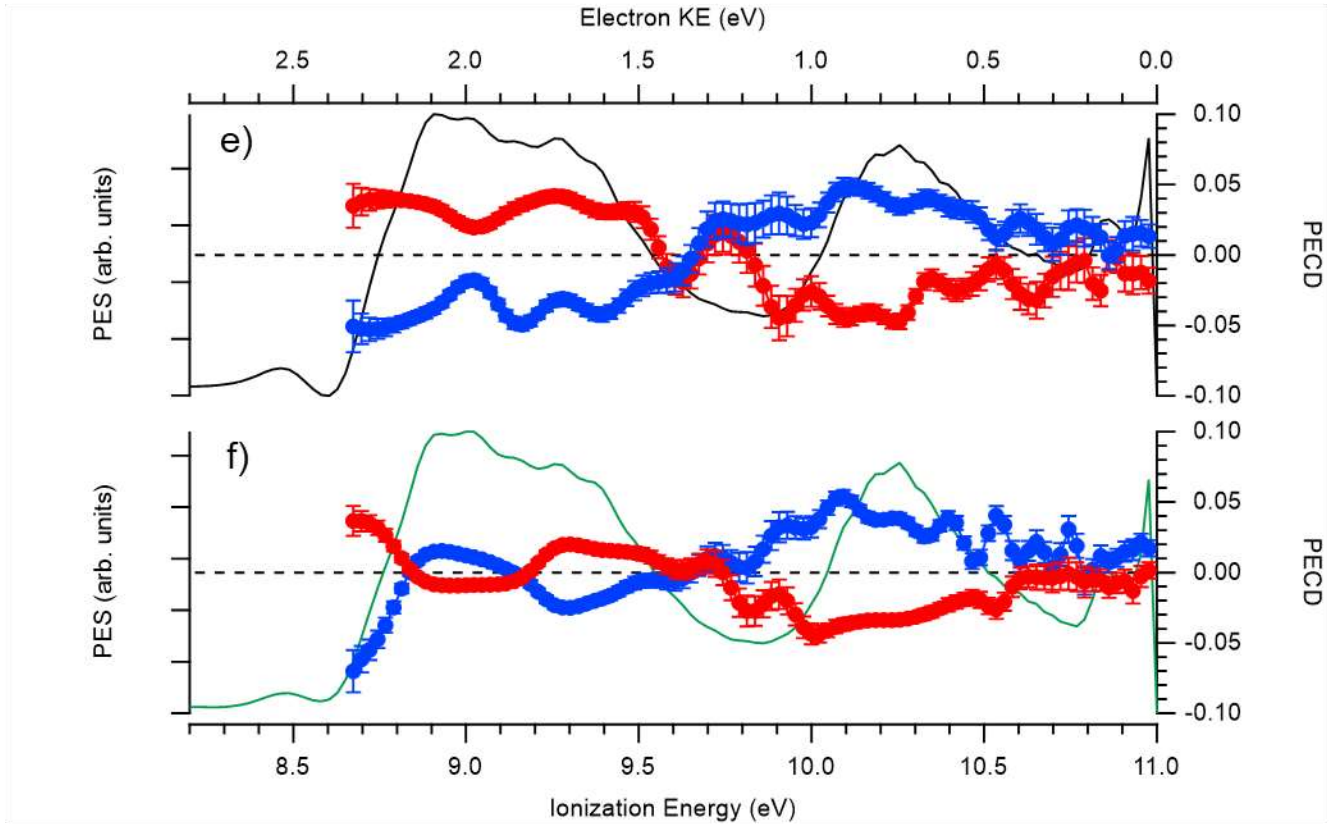
Electron KE (eV)
e)
f)
PES (arb. units)
PECD
Ionization Energy (eV)

Figure 3: PES and dichroic parameter at 11 eV. Raw (half left) and Abel-inverted (half right) difference images (LCPL –RCPL), of the photoelectron distribution: data in argon for (*R*) 1-indanol (a), (*S*) 1-indanol (b) and in helium for (*R*) 1-indanol (c) and (*S*) 1-indanol (d). The photon beam propagates from the top to the bottom of the images as indicated by the arrow. PES (solid lines) and PECD curves (solid circles) in Ar (e) and He (f) for the (*S*) (red) and (*R*) enantiomers (blue).

The same experiment was performed at a photon energy of 12 eV (see Figure S5). The dependence of PECD upon conformation is much less striking at 12 eV and the signal shows identical sign and similar magnitude in helium and in argon, except in the region of the HOMO-2 where clear differences are observed.

These results evidence the expected strong dependence of the PECD upon the ionized orbital and the electron kinetic energy. This is further highlighted in Figure 4, which displays the mean PECD values, recorded between 9 and 12 eV, of the (*S*) enantiomer for the three highest occupied orbitals as a function of the electron kinetic energy. The b_1 values, obtained following the procedure described in the SI (Figures S6 and S7), depend on both the electron kinetic energy and the carrier gas (see Figure 4). At low electron kinetic energy (< 1.2 eV), b_1 is the same for the two carrier gases, whatever the orbital considered. A strong similitude between the two carrier gases is also observed at electron kinetic energy > 2.5 eV. This indicates that the PECD is not sensitive to conformational isomerism in these electron kinetic energy ranges. In contrast, the behavior of the PECD is dramatically different for intermediate electron kinetic energies, between 1.5 and 2.5 eV. There, the measured b_1 parameters clearly differ from each other. This observation holds for the three highest occupied orbitals. At 1.7 eV, the PECD is of identical sign for either of the carrier

gases, but of larger magnitude in argon. This indicates that the PECD of 2ax has opposite direction relative to that of 1eq, although not intense enough to counterbalance the effect of the latter and invert the sign of the total PECD. The most striking effect is observed for the HOMO at 2.1 eV, for which the PECD changes sign when changing the carrier gas, showing unambiguously that the PECD are opposite in sign for the two conformers. Moreover, the magnitude of the PECD of 2ax is large enough to counterbalance the opposite effect of the most abundant 1eq conformer, which results in an inversion in the sign of the total PECD. We can also observe in Figure 4 that the strongest PECDs are obtained for the HOMO-2 orbital localized on the oxygen lone pair in both carrier gases. This orbital is adjacent to the chiral center, which is also the locus of conformational isomerism.

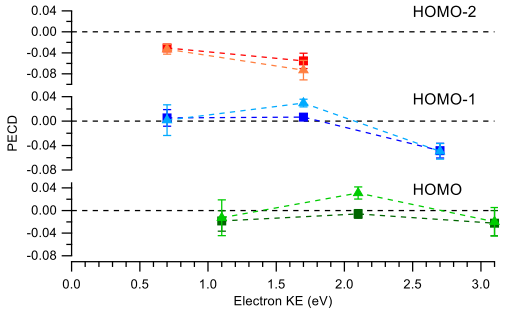

Figure 4: Mean values of the PECD weighed by the PES intensity over their respective FWHM, as described in the SI, of the three highest occupied orbitals HOMO to HOMO-2, corresponding to the X, A and B band, for (S) 1-indanol in helium (squares) and in argon (triangles) as a function

of the electron kinetic energy. The error bars are calculated using the maximum PECD error in the area corresponding to the X, A and B bands, according to the procedure described in the SI. These data have been obtained at 10, 11 and 12 eV photon energy (except for the HOMO-2 where they were obtained only at 11 and 12 eV).

Overall, and in contrast to the photoelectron spectra and anisotropy parameter β, the PECD is dramatically sensitive to minute differences in the molecular structure. Indeed, the outgoing photoelectron is represented as a linear combination of partial spherical waves that are scattered by the molecular potential, leading to changes in their relative amplitude and phases, which are eventually mapped into the photoionization observables written in equation 1. The orbital cross-sections contributing to the PES (also known as b_0) have no phase dependency while b_2 is partially proportional to the cosine of the relative phase between every other partial waves. In contrast, b_1 is fully proportional to the sine of the phase differences between adjacent partial waves,[14] and therefore will be more sensitive to small phase changes (in magnitude and sign) induced by subtle differences in the chiral molecular potential. The effect of conformational isomerism is evidenced for low, but non-zero, electron kinetic energy, between 1.5 and 2 eV. Typically in this slow electron energy range (0-4 eV), PECD has been shown experimentally and theoretically to be very sensitive to isomerism and chemical substitution[20 40], as well as conformations.[19 26 27] The strong sensitivity of PECD to structural parameters at low kinetic energy can be intuitively rationalized in the context of electron scattering, where slow photoelectrons will be more sensitive to the scattering potential and therefore to the fine details of the molecular structure.[41] Also within this context, it has been shown that the chiral parameter b_1, unlike β and the PES, is the only scattering parameter fully dependent on the phase shifts imprinted by the molecular potential onto the electronic outgoing partial waves.[14] The sensitivity of PECD to conformation is especially

apparent for the ionization of the HOMO and an electron kinetic energy of 2.1 eV, where b_1 is opposite in sign for 1eq and 2ax, with a four-fold larger value for the latter. Although the effect is especially pronounced for the HOMO, it appears also to a lesser extent for HOMO-1 and HOMO-2. The strongest PECD is observed for the HOMO-2 orbital localized on the oxygen lone pair, which is adjacent to the chiral center. Despite the chiral center being also the locus of conformational isomerism, HOMO-2 is less sensitive to conformational isomerism than HOMO and HOMO-1, located on the aromatic ring, thus further from the chiral center. The larger sensitivity of the diffuse π orbitals demonstrates the non-local character of chirality and the subtle effect of both the initial state and the intrinsically chiral potential scattering off the departing electron. Other chiroptical spectroscopy methods, like vibrational circular dichroism (VCD), have proven the non-locality of chirality.[42] In the case of 1-indanol in particular, a dramatic difference in magnitude and sign of the VCD signal has been observed for the equatorial and axial conformers, even for vibrations localized far from the chiral center. [6, 8]

The present results prove the exquisite conformational sensitivity of PECD, in a case where the PES as well as the β parameter, despite its reported sensitivity to the orbital character and hybridization,[43] are genuinely superimposable. Such a situation is quite common, so that the outcome of this study may have strong consequences for the ongoing development on laser-based PECD techniques in an analytical context. The determination of enantiomeric excess of a given chiral species or mixture of species determined by such techniques might be skewed by the presence of several conformations.[44 45 46 21-23] Special attention should thus be paid to the possible existence of conformers, and the conformational landscape should be carefully explored before applying PECD to analytical purposes and comparing experimental values to simulations.[41] In this applied context, but for fundamental motivations as well, the present work paves the way for

conformer-selective PECD measurements. These measurements are based on a resonance-enhanced multi-photon ionization (REMPI) scheme with high resolution ns lasers, currently in progress in our group, for which the effects of conformational isomerism on higher-order odd coefficients like b_3[47] will also be explored, as well as the influence of the formation of diastereomer complexes on PECD.[48-49]

Experimental Methods

The experiments were performed at the beamline DESIRS of the French national synchrotron facility SOLEIL. This undulator-based beamline allows obtaining tuneable polarization-controlled vacuum ultraviolet (VUV) radiation, with an absolute circular polarization rate above 97%.[50] It is equipped with the dedicated SAPHIRS set-up that encompasses a continuous supersonic expansion and the i^{2}PEPICO DELICIOUS3 double imaging spectrometer, described earlier, which allows detection of electrons and ions in coincidence.[51]

Commercially-available (Sigma-Aldrich) enantiopure samples of either (*S*)-(+) or (*R*)-(-)-1-indanol were brought into the gas phase by resistive heating in an oven at 75 °C and expanded through a 200 µm nozzle, using either helium at a backing pressure of 0.5 bar or argon at a backing pressure of 0.1 bar as a carrier gas. The resulting supersonic expansion was passed through a double skimmer and crossed the synchrotron light in the spectrometer chamber. The formed ions and electrons were accelerated in opposite directions and detected in coincidence by a modified Wiley - McLaren imaging time of flight (TOF) spectrometer and a velocity map imaging (VMI) detector, respectively.

For a given enantiomer seeded in a given carrier gas, between 20 and 50 successive files accumulated for 10 mn each were recorded with alternating light helicity, to minimize the effect of the long-term fluctuations on the signal. The corresponding raw electron images were filtered

for the mass of the parent (*m/z* 134) and that of the fragment resulting from hydrogen loss (*m/z* 133). The sum (LCPL+RPCL) image file, after Abel-inversion via the pBasex software,[52] provided the PES and the b_2 parameter, while the difference image file (LCPL-RCPL) provided the b_1 parameter and therefore the PECD= $2b_1$, according to a procedure already described.[53] The p-Basex software is based on the Abel transform of the electron distribution and aims at reconstructing the three-dimensional Newton sphere of the expanding electrons from its two-dimensional projection. It consists of fitting a set of polar basis functions with a known and exact inverse Abel function. The error bars were estimated assuming a Poisson distribution of the image pixel intensities and propagating the Poisson standard deviation through the image inversion transformation. The PES spectra were fitted by Gaussian functions to disentangle the contributions of the different highest occupied orbitals. The procedure is detailed in Figures 6 and 7 of the SI (Section 3). The dependence of PECD upon electron kinetic energy was deduced from the experimental data by integrating b_1 over the simulated curve corresponding to each highest occupied orbital. Such experiments were performed at several photon energies between 9 and 12 eV. Threshold-Photoelectron Spectra (TPES) and mass-selected TPES (TPEPICO) were also measured by recording the near zero kinetic energy electron counts at a typical electron resolution of 20 meV.[54]

Theoretical methods

The two most stable conformational isomers observed under supersonic jet conditions, namely, equatorial (1eq) and axial (2ax), were considered in the calculations.[30] The used nomenclature is identical to that of former works.[32-33] The structures previously obtained at the B3LYP-D3BJ/6-31++G(d,p) level were re-optimized at the MP2/6-31++G(d,p) level. Both vertical and adiabatic ionization energies (IE) were determined. The electronic densities were calculated at the MP2 level

of theory and the cube files were generated using the cubegen facility implemented in the Gaussian software, version G16 B01.[55] The isodensity was plotted for each occupied orbital from HOMO to HOMO-3 using the VMD software, with an isodensity value of 0.04.[56] Energies of the valence orbitals were calculated using the outer valence Green's function (OVGF) method and cc-pVTZ basis set, at the MP2/6-31G++(d,p) optimized geometries.[57-58]

ASSOCIATED CONTENT

Supporting Information. The following file is available free of charge. It contains additional experimental results (mass spectra, PES, b_2 parameters and PECD recorded at a photon energy of 11 eV, TPES), the procedure for extracting the b_1 parameters of different orbitals, and theoretical results (Conformers energies for different theoretical methods)
(SupportingInformationPECD.pdf)

AUTHOR INFORMATION

The authors declare no competing financial interests.

Corresponding Authors:
Anne Zehnacker anne.zehnacker-rentien@universite-paris-saclay.fr Laurent Nahon laurent.nahon@synchrotron-soleil.fr

ACKNOWLEDGMENT

This work has been supported by the program "Investissements d'Avenir LabEx PALM" (ANR-10-LABX-0039-PALM). The authors are grateful to the SOLEIL general staff for providing synchrotron beam under proposals No. 20181193 and 20200234. We acknowledge the

computing center MésoLUM managed by ISMO (UMR8214) and LPGP (UMR8578), University Paris-Saclay (France). We thank Prof. Ivan Powis for helpful discussions and suggestions.

REFERENCES

1. Berova, N.; Nakanishi, K.; Woody, R. W. *Circular Dichroism. Principle and Applications*. Wiley: New York, 2000.
2. Berova, N.; Di Bari, L.; Pescitelli, G. Application of electronic circular dichroism in configurational and conformational analysis of organic compounds. *Chemical Society Reviews* **2007,** *36* (6), 914-931.
3. Mendonca, L.; Hache, F.; Changenet-Barret, P.; Plaza, P.; Chosrowjan, H.; Taniguchi, S.; Imamoto, Y. Ultrafast Carbonyl Motion of the Photoactive Yellow Protein Chromophore Probed by Femtosecond Circular Dichroism. *Journal of the American Chemical Society* **2013,** *135* (39), 14637-14643.
4. He, Y.; Bo, W.; Dukor, R. K.; Nafie, L. A. Determination of Absolute Configuration of Chiral Molecules Using Vibrational Optical Activity: A Review. *Applied Spectroscopy* **2011,** *65* (7), 699-723.
5. Merten, C. Recent Advances in the Application of Vibrational Circular Dichroism Spectroscopy for the Characterization of Asymmetric Catalysts. *European Journal of Organic Chemistry* **2020,** *2020* (37), 5892-5900.
6. Johnson, J. L.; Polavarapu, P. L. Chiral Molecular Structures of Substituted Indans: Ring Puckering, Rotatable Substituents, and Vibrational Circular Dichroism. *Acs Omega* **2019,** *4* (3), 4963-4976.
7. Keiderling, T. A. Structure of Condensed Phase Peptides: Insights from Vibrational Circular Dichroism and Raman Optical Activity Techniques. *Chemical Reviews* **2020,** *120* (7), 3381-3419.
8. Le Barbu-Debus, K.; Scherrer, A.; Bouchet, A.; Sebastiani, D.; Vuilleumier, R.; Zehnacker, A. Effect of puckering motion and hydrogen bond formation on the vibrational circular dichroism spectrum of a flexible molecule: the case of (S)-1-indanol. *Physical Chemistry Chemical Physics* **2018,** *20* (21), 14635-14646.
9. Jahnigen, S.; Zehnacker, A.; Vuilleumier, R. Computation of Solid-State Vibrational Circular Dichroism in the Periodic Gauge. *Journal of Physical Chemistry Letters* **2021,** *12* (30), 7213-7220.
10. Le Barbu-Debus, K.; Bowles, J.; Jahnigen, S.; Clavaguera, C.; Calvo, F.; Vuilleumier, R.; Zehnacker, A. Assessing cluster models of solvation for the description of vibrational circular dichroism spectra: synergy between static and dynamic approaches. *Physical Chemistry Chemical Physics* **2020,** *22* (45), 26047-26068.
11. Hong, A.; Choi, C. M.; Eun, H. J.; Jeong, C.; Heo, J.; Kim, N. J. Conformation-Specific Circular Dichroism Spectroscopy of Cold, Isolated Chiral Molecules. *Angewandte Chemie-International Edition* **2014,** *53* (30), 7805-7808.
12. Hong, A.; Jeong, C.; Jang, H.; Choi, M. C.; Heo, J.; Kim, N. J. Fluorescence-detected circular dichroism spectroscopy of jet-cooled ephedrine. *Physical Chemistry Chemical Physics* **2016,** *18* (11), 7762-7767.

13. Eun, H. J.; Min, A.; Jeon, C. W.; Yoo, I. T.; Heo, J.; Kim, N. J. Chiral and Isomeric Discrimination of Chiral Molecular Ions by Cold Ion Circular Dichroism Spectroscopy. *Journal of Physical Chemistry Letters* **2020,** *11* (11), 4367-4371.
14. Powis, I. Photoelectron circular dichroism in chiral molecules. In *Advances in Chemical Physics, Vol 138*, Rice, S. A., Ed. 2008; Vol. 138, pp 267-329.
15. Nahon, L.; Garcia, G. A.; Powis, I. Valence shell one-photon photoelectron circular dichroism in chiral systems. *Journal of Electron Spectroscopy and Related Phenomena* **2015,** *204*, 322-334.
16. Hadidi, R.; Bozanic, D. K.; Garcia, G. A.; Nahon, L. Electron asymmetries in the photoionization of chiral molecules: possible astrophysical implications. *Advances in Physics-X* **2018,** *3* (1), 833-861.
17. Ganjitabar, H.; Hadidi, R.; Garcia, G. A.; Nahon, L.; Powis, I. Vibrationally-resolved photoelectron spectroscopy and photoelectron circular dichroism of bicyclic monoterpene enantiomers. *Journal of Molecular Spectroscopy* **2018,** *353*, 11-19.
18. Hadidi, R.; Božanić, D. K.; Ganjitabar, H.; Garcia, G. A.; Powis, I.; Nahon, L. Conformer-dependent vacuum ultraviolet photodynamics and chiral asymmetries in pure enantiomers of gas phase proline. *Communications Chemistry* **2021,** *4* (1), 72-.
19. Tia, M.; de Miranda, B. C.; Daly, S.; Gaie-Levrel, F.; Garcia, G. A.; Powis, I.; Nahon, L. Chiral Asymmetry in the Photoionization of Gas-Phase Amino-Acid Alanine at Lyman-alpha Radiation Wavelength. *Journal of Physical Chemistry Letters* **2013,** *4* (16), 2698-2704.
20. Nahon, L.; Nag, L.; Garcia, G. A.; Myrgorodska, I.; Meierhenrich, U.; Beaulieu, S.; Wanie, V.; Blanchet, V.; Geneaux, R.; Powis, I. Determination of accurate electron chiral asymmetries in fenchone and camphor in the VUV range: sensitivity to isomerism and enantiomeric purity. *Physical Chemistry Chemical Physics* **2016,** *18* (18), 12696-12706.
21. Kastner, A.; Lux, C.; Ring, T.; Zullighoven, S.; Sarpe, C.; Senftleben, A.; Baumert, T. Enantiomeric Excess Sensitivity to Below One Percent by Using Femtosecond Photoelectron Circular Dichroism. *ChemPhysChem* **2016,** *17* (8), 1119-1122.
22. Fanood, M. M. R.; Ram, N. B.; Lehmann, C. S.; Powis, I.; Janssen, M. H. M. Enantiomer-specific analysis of multi-component mixtures by correlated electron imaging-ion mass spectrometry. *Nature Communications* **2015,** *6*, 7511-.
23. Comby, A.; Bloch, E.; Bond, C. M. M.; Descamps, D.; Miles, J.; Petit, S.; Rozen, S.; Greenwood, J. B.; Blanchet, V.; Mairesse, Y. Real-time determination of enantiomeric and isomeric content using photoelectron elliptical dichroism. *Nature Communications* **2018,** *9*, 5212-.
24. Comby, A.; Beaulieu, S.; Boggio-Pasqua, M.; Descamps, D.; Legare, F.; Nahon, L.; Petit, S.; Pons, B.; Fabre, B.; Mairesse, Y.; Blanchett, V. Relaxation Dynamics in Photoexcited Chiral Molecules Studied by Time-Resolved Photoelectron Circular Dichroism: Toward Chiral Femtochemistry. *Journal of Physical Chemistry Letters* **2016,** *7* (22), 4514-4519.
25. Blanchet, V.; Descamps, D.; Petit, S.; Mairesse, Y.; Pons, B.; Fabre, B. Ultrafast relaxation investigated by photoelectron circular dichroism: an isomeric comparison of camphor and fenchone. *Physical Chemistry Chemical Physics* **2021,** *23* (45), 25612-25628.
26. Turchini, S. Conformational effects in photoelectron circular dichroism. *Journal of Physics-Condensed Matter* **2017,** *29* (50), 503001-.
27. Daly, S.; Tia, M.; Garcia, G. A.; Nahon, L.; Powis, I. The Interplay Between Conformation and Absolute Configuration in Chiral Electron Dynamics of Small Diols. *Angewandte Chemie-International Edition* **2016,** *55* (37), 11054-11058.
28. Hartweg, S.; Garcia, G. A.; Bozanic, D. K.; Nahon, L. Condensation Effects on Electron Chiral Asymmetries in the Photoionization of Serine: From Free Molecules to Nanoparticles. *Journal of Physical Chemistry Letters* **2021,** *12* (9), 2385-2393.

29. Scuderi, D.; Paladini, A.; Satta, M.; Catone, D.; Piccirillo, S.; Speranza, M.; Guidoni, A. G. Chiral aggregates of indan-1-ol with secondary alcohols and water: Laser spectroscopy in supersonic beams. *Physical Chemistry Chemical Physics* **2002,** *4* (20), 4999-5003.
30. Le Barbu-Debus, K.; Lahmani, F.; Zehnacker-Rentien, A.; Guchhait, N.; Panja, S. S.; Chakraborty, T. Fluorescence spectroscopy of jet-cooled chiral (+/-)-indan-1-ol and its cluster with (+/-)-methyl- and ethyl-lactate. *Journal of Chemical Physics* **2006,** *125* (17), 174305.
31. Velino, B.; Ottaviani, P.; Caminati, W.; Giardini, A.; Paladini, A. Conformational landscapes and free-jet rotational spectrum of indan-1-ol. *ChemPhysChem* **2006,** *7* (3), 565-568.
32. Bouchet, A.; Altnoder, J.; Broquier, M.; Zehnacker, A. IR-UV spectroscopy of jet-cooled 1-indanol: Restriction of the conformational space by hydration. *Journal of Molecular Structure* **2014,** *1076*, 344-351.
33. Hernandez-Castillo, A. O.; Bischoff, J.; Lee, J. H.; Langenhan, J.; Karra, M.; Meijer, G.; Eibenberger-Arias, S. High-resolution UV spectroscopy of 1-indanol. *Physical Chemistry Chemical Physics* **2021,** *23* (12), 7048-7056.
34. Das, A.; Mahato, K. K.; Panja, S. S.; Chakraborty, T. Conformations of indan and 2-indanol: A combined study by UV laser spectroscopy and quantum chemistry calculation. *Journal of Chemical Physics* **2003,** *119* (5), 2523-2530.
35. Pachner, K.; Steglich, M.; Hemberger, P.; Fischer, I. Photodissociation dynamics of the ortho- and para-xylyl radicals. *Journal of Chemical Physics* **2017,** *147* (8), 084303-.
36. Altnoeder, J.; Bouchet, A.; Lee, J. J.; Otto, K. E.; Suhm, M. A.; Zehnacker-Rentien, A. Chirality-dependent balance between hydrogen bonding and London dispersion in isolated (+-)-1-indanol clusters. *Physical Chemistry Chemical Physics* **2013,** *15*, 10167-10180.
37. He, Y.; Kong, W. Resonantly enhanced multiphoton ionization and zero kinetic energy photoelectron spectroscopy of 2-indanol conformers. *Journal of Chemical Physics* **2006,** *124* (20), 204306-.
38. Matsuda, Y.; Harigaya, H.; Xie, M.; Takahashi, K.; Fujii, A. Infrared spectroscopic investigations of cationic ethanol, propanol, and butanol. *Chemical Physics Letters* **2015,** *640*, 215-218.
39. Garcia, G. A.; Nahon, L.; Daly, S.; Powis, I. Vibrationally induced inversion of photoelectron forward-backward asymmetry in chiral molecule photoionization by circularly polarized light. *Nature Communications* **2013,** *4*, 2132-.
40. Garcia, G. A.; Dossmann, H.; Nahon, L.; Daly, S.; Powis, I. Photoelectron circular dichroism and spectroscopy of trifluoromethyl- and methyl-oxirane: a comparative study. *Physical Chemistry Chemical Physics* **2014,** *16* (30), 16214-16224.
41. Tia, M.; de Miranda, B. C.; Daly, S.; Gaie-Levrel, F.; Garcia, G. A.; Nahon, L.; Powis, I. VUV Photodynamics and Chiral Asymmetry in the Photoionization of Gas Phase Alanine Enantiomers. *Journal of Physical Chemistry A* **2014,** *118* (15), 2765-2779.
42. Jähnigen, S.; Scherrer, A.; Vuilleumier, R.; Sebastiani, D. Chiral Crystal Packing Induces Enhancement of Vibrational Circular Dichroism. *Angewandte Chemie-International Edition* **2018,** *57* (40), 13344-13348.
43. Signorell, R.; Yoder, B. L.; West, A. H. C.; Ferreiro, J. J.; Saak, C.-M. Angle-resolved valence shell photoelectron spectroscopy of neutral nanosized molecular aggregates. *Chemical Science* **2014,** *5* (4), 1283-1295.
44. Miles, J.; Fernandes, D.; Young, A.; Bond, C. M. M.; Crane, S. W.; Ghafur, O.; Townsend, D.; Sa, J.; Greenwood, J. B. A new technique for probing chirality via photoelectron circular dichroism. *Analytica Chimica Acta* **2017,** *984*, 134-139.
45. Janssen, M. H. M.; Powis, I. Direct Enantiomer-Selective Mass Spectrometry of Chiral Mixtures by Mass-Selected Photoelectron Circular Dichroism. *Spectroscopy on line* **2017,** *15* (2), 16-23.

46. Lehmann, C. S.; Weitzel, K. M. Coincident measurement of photo-ion circular dichroism and photo-electron circular dichroism. *Phys. Chem. Chem. Phys.* **2020,** *22* (24), 13707-13712.
47. Kastner, A.; Koumarianou, G.; Glodic, P.; Samartzis, P.; Ladda, N.; Ranecky, S. T.; Ring, T.; Sudheendran, V.; Witte, C.; Braun, H.; Lee, H. G.; Senftleben, A.; Berger, R.; Park, G. B.; Schafer, T.; Baumert, T. High-resolution resonance-enhanced multiphoton photoelectron circular dichroism. *Physical Chemistry Chemical Physics* **2020,** *22* (14), 7404-7411.
48. Zehnacker, A. Chirality Effects in Gas-Phase Spectroscopy and Photophysics of Molecular and Ionic Complexes: Contribution of Low and Room Temperature Studies. *International Reviews in Physical Chemistry* **2014,** *33* (2), 151-207.
49. Zehnacker, A.; Suhm, M. A. Chirality recognition between neutral molecules in the gas phase. *Angewandte Chemie-International Edition* **2008,** *47* (37), 6970-6992.
50. Nahon, L.; de Oliveira, N.; Garcia, G. A.; Gil, J. F.; Pilette, B.; Marcouille, O.; Lagarde, B.; Polack, F. DESIRS: a state-of-the-art VUV beamline featuring high resolution and variable polarization for spectroscopy and dichroism at SOLEIL. *Journal of Synchrotron Radiation* **2012,** *19*, 508-520.
51. Garcia, G. A.; de Miranda, B. K. C.; Tia, M.; Daly, S.; Nahon, L. DELICIOUS III: A multipurpose double imaging particle coincidence spectrometer for gas phase vacuum ultraviolet photodynamics studies. *Review of Scientific Instruments* **2013,** *84* (5), 053112-.
52. Garcia, G. A.; Nahon, L.; Powis, I. Two-dimensional charged particle image inversion using a polar basis function expansion. *Review of Scientific Instruments* **2004,** *75* (11), 4989-4996.
53. Nahon, L.; Garcia, G. A.; Harding, C. J.; Mikajlo, E.; Powis, I. Determination of chiral asymmetries in the valence photoionization of camphor enantiomers by photoelectron imaging using tunable circularly polarized light. *Journal of Chemical Physics* **2006,** *125* (11), 114309-.
54. Garcia, G. A.; Soldi-Lose, H.; Nahon, L. A versatile electron-ion coincidence spectrometer for photoelectron momentum imaging and threshold spectroscopy on mass selected ions using synchrotron radiation. *Review of Scientific Instruments* **2009,** *80*, 023102.
55. Frisch, M. J.; Trucks, G. W.; Schlegel, H. B.; Scuseria, G. E.; Robb, M. A.; Cheeseman, J. R.; Scalmani, G.; Barone, V.; Petersson, G. A.; Nakatsuji, H.; Li, X.; Caricato, M.; Marenich, A. V.; Bloino, J.; Janesko, B. G.; Gomperts, R.; Mennucci, B.; Hratchian, H. P.; Ortiz, J. V.; Izmaylov, A. F.; Sonnenberg, J. L.; Williams; Ding, F.; Lipparini, F.; Egidi, F.; Goings, J.; Peng, B.; Petrone, A.; Henderson, T.; Ranasinghe, D.; Zakrzewski, V. G.; Gao, J.; Rega, N.; Zheng, G.; Liang, W.; Hada, M.; Ehara, M.; Toyota, K.; Fukuda, R.; Hasegawa, J.; Ishida, M.; Nakajima, T.; Honda, Y.; Kitao, O.; Nakai, H.; Vreven, T.; Throssell, K.; Montgomery Jr., J. A.; Peralta, J. E.; Ogliaro, F.; Bearpark, M. J.; Heyd, J. J.; Brothers, E. N.; Kudin, K. N.; Staroverov, V. N.; Keith, T. A.; Kobayashi, R.; Normand, J.; Raghavachari, K.; Rendell, A. P.; Burant, J. C.; Iyengar, S. S.; Tomasi, J.; Cossi, M.; Millam, J. M.; Klene, M.; Adamo, C.; Cammi, R.; Ochterski, J. W.; Martin, R. L.; Morokuma, K.; Farkas, O.; Foresman, J. B.; Fox, D. J. *Gaussian 16 Rev. B.01*, Wallingford, CT, 2016.
56. Humphrey, W.; Dalke, A.; Schulten, K. VMD - Visual Molecular Dynamics. *J. Molec. Graphics* **1996,** *14*, 33-38.
57. Vonniessen, W.; Schirmer, J.; Cederbaum, L. S. Computational methods for the one-particle Green-function. *Computer Physics Reports* **1984,** *1* (2), 57-125.
58. Garcia, G. A.; Nahon, L.; Harding, C. J.; Powis, I. Chiral signatures in angle-resolved valence photoelectron spectroscopy of pure glycidol enantiomers. *Physical Chemistry Chemical Physics* **2008,** *10* (12), 1628-1639.